Enhanced mechanical and tribological properties of low-cost core-shell structured microcrystalline graphite/Cu composites

Min Zhong[1a], Shengzhi Duan[1a], Xiaowen Wu[1,*], Xin Min[1], Zhaohui Huang[1], Minghao Fang[1], Huanxin Li[2], Hao Ding[1,*], Bingcheng Luo[3,*]

[1]Engineering Research Center of Ministry of Education for Geological Carbon Storage and Low Carbon Utilization of Resources, Beijing Key Laboratory of Materials Utilization of Nonmetallic Minerals and Solid Wastes, National Laboratory of Mineral Materials, School of Materials Science and Technology, China University of Geosciences (Beijing), 100083, China

[2]Department of Chemistry, Physical & Theoretical Chemistry Laboratory, University of Oxford, South Parks Road, Oxford OX1 3QZ, United Kingdom

[3]College of Science, China Agricultural University, Beijing 100083, China.

Min Zhong and Shengzhi Duan contributed equally to this work. (co-first author)

*Corresponding author. Email address: xwwu@cugb.edu.cn (X. Wu);

dinghao@cugb.edu.cn (H. Ding); luobc21@cau.edu.cn (B. Luo)

Abstract: In the past, microcrystalline graphite (MG) was mainly used for the preparation of carbon enhancers and flame retardant, and is a low value-added inorganic mineral. There are very few reports of microcrystalline graphite being compounded with Cu to produce friction materials. Carbon coated microcrystalline graphite/Cu (Carbon@MG/Cu) composites were prepared by coating microcrystalline graphite with phenolic resin and mixing it with Cu. The effect of the phenolic resin coating on the

1

mechanical and tribological properties of the composites was investigated by comparison with pure Cu, microcrystalline graphite/Cu (MG/Cu). The hardness and flexural strength of pure Cu were 39.8 HV and 72.3 MPa, respectively. The protection of the amorphous carbon shells led to a significant improvement in the mechanical properties of Carbon@MG/Cu, with hardness and flexural strengths of 72.3 HV and 103.8 MPa. The poor bonding between the MG and Cu severely affects its mechanical properties. Pure Cu has the highest wear rate $(10.6 \times 10^{-7}(\text{mm}^3/(\text{N·m}))$, while Carbon@MG/Cu has a stable coefficient of friction (0.19) and the lowest wear rate (4.3 x 10^{-7} (mm^3 /(N·m))) compared to pure Cu and MG/Cu. We provide a method to prepare graphite/copper composites with high mechanical and tribological properties based on low-cost microcrystalline graphite, which helps to solve the problem of reuse of microcrystalline graphite and increase its industrial added value.

Keywords: Carbon-coated microcrystalline graphite/Cu; Tribological properties; Solid self-lubrication; Powder metallurgy;

1. Introduction

China is the world's leading producer of graphite with a market share of nearly 66%, and both flake graphite and MG reserves are among the highest in the world[1] In the past, MG was mainly used for making pencils and carbon enhancers and was a low value-added inorganic mineral. In some areas of China, it was even used for combustion, which would have resulted in a huge waste of resources. At present, the utilization rate of MG in China is low, and many enterprises sell the high-grade raw ore directly or sell the raw ore after primary processing, which will lead to a low return on

resources. Over the past half century, flake graphite has been added to copper-based materials as a solid lubricant to improve their frictional wear and electrical conductivity, and is widely used as friction materials such as brushes, electrical contacts, and brake cartridges, etc.[2-4]. However, as flake graphite resources are decreasing, MG is becoming more and more important due to its abundance[5]. More importantly, the price of MG is only half or one-third of that of flake graphite[6]. Currently, research on MG has focused on battery cathodes, isotropic graphite and graphene. In contrast, the preparation of electrical sliding contact and friction materials by compounding with copper has rarely been reported.

At high speeds, the pantograph slider and the contact wire will be subjected to severe friction, which is a major challenge for the mechanical and tribological properties of graphite/Cu pantograph sliders[7]. Both graphite and copper have poor wettability, and when graphite is embedded in a Cu matrix, graphite and Cu can only form a mechanical interlock[8]. When graphite/Cu composites are subjected to strong mechanical shock and arc heat, cracks will develop and expand at the Cu-carbon interface, which shortens the life of the material and even causes it to fail. These factors limit the practical application of graphite/Cu composites[4, 9].Many methods have been proposed to improve the bonding of graphite-Cu interface. On the one hand, the addition of alloy additives such as Cr, Ti and V are prone to carbide formation[11]. Electroplating metal layers (Cu, Ni[10, 11]) on graphite surface is also one of the most effective ways to improve the weak interfacial bonding, such as plasma deposition, physical vapor deposition[12], chemical vapor deposition, electroplating and chemical

plating[13-15]. Wang[16] et al. studied the effects of chemical silver plating over graphite on the microstructure and mechanical properties of Cu-Ni-graphite composites. The results showed that silver particles on the graphite surface modified the Cu-Ni-graphite interface, forming silver nanowires and α-Cu phases at the leading edge of the matrix and graphite, which improved the interfacial strength and mechanical properties. Chen[17] used chemical nickel plating to improve the bonding of the interface between graphite and copper. However, the process of plating metal on graphite surfaces is complex, costly and environmentally unfriendly.

In order to further increase the mechanical and tribological properties of low-cost MG/Cu composites, we prepared a core-shell structure of resin-coated carbon composite with Cu matrix by coating MG with phenolic resin inspired by pioneering work[20]. Here we use MG to reduce the cost of preparing copper-based friction composites, improve the utilization of MG ore and increase the industrial value of microcrystalline graphite. We further and set up a control group to investigate the effect of carbon coated MG(Carbon@MG) as well as untaken carbon coated MG on the mechanical and tribological properties of the composites, in contrast to pure Cu. We provide a method for the preparation of graphite/Cu composites with high mechanical and tribological properties based on low-cost microcrystalline graphite, which helps to address the reuse of microcrystalline graphite and increase its industrial added value.

2. Experimental

2.1 Preparation of Carbon@MG

Carbon@MG was prepared by liquid-phase impregnation evaporation solvent carbonization method. The average particle size of 38 μm microcrystalline graphite (MG, 99% purity, Hebei, China, also Eagle Welding Materials Ltd.) and phenolic resin powder (PR 2123 powder, softening point 95-110°C, 3.0-4.0% free phenol, Henan Jieyang New Materials Co., Ltd.) were used as the raw materials.

Fig. 1 illustrates the preparation of Carbon@MG. Firstly, 25% of PR was dissolved in ethanol and ultrasonically dissolved for 5min, then 75% of MG was added and ultrasonically dispersed for 5min, then the phenolic resin solution was put into an electric blast drying oven to evaporate the alcohol and will dry the solid. Finally, the phenolic resin carbon coated microcrystalline graphite (PR@MG) is obtained by crushing and sieving. Carbon@MG was obtained by heating the PR@MG at 900°C for 2 hours under hydrogen.
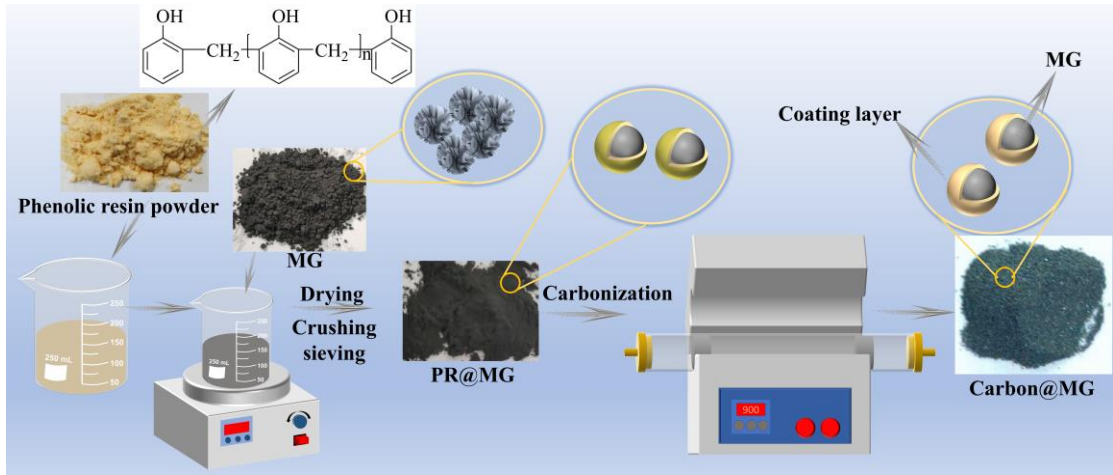
Figure 1. The schematic illustration of preparation of Carbon@MG.

2.2 Preparation of microcrystalline graphite/Cu composites

In summary, three samples were prepared. They were pure Cu, MG/Cu and Carbon@MG/Cu. Commercially available microcrystalline graphite (10wt%),

PR@MG (10wt%) and electrolytic Cu powder (90wt%, average particle size 40μm, Shenzhen Sujia Technology Co., Ltd.) were used in this study. Three samples of pure Cu, MG/Cu and Carbon@MG/Cu were prepared respectively. The preparation procedures of the samples were as follows:

The samples were manufactured by using powder metallurgy. Firstly, electrolytic Cu powder (90 wt %) was mixed with MG (10 wt %) or Carbon@MG (10 wt %) in a mortar and pestle with appropriate amount of alcohol for 1 h, and then electrolytic Cu powder (90 wt %) was dry-mixed with MG (10 wt %) or Carbon@MG (10 wt %) for 2 h using a powder mixer, Rotation speed of 30 rpm. Next, cold pressing was carried out at 300MPa unidirectional pressure for 3 min using a compression molding machine. Then, vacuum sintering was carried out at 900°C for 1 h in a hydrogen atmosphere with a heating rate of 8 °C/min.

2.3 Characterization

The relative density of the composites was measured using the drainage method. Crystal structures of MG and Carbon@MG were analyzed with the aid of an X-ray diffractometer (XRD, D/MAX-Ultima IV) using Cu Kα radiation varying from 10° to 80° at a rate of 10°/min. A SUPRA-55 scanning electron microscope (SEM, vacuum of 10^{-5} Pa, accelerating voltage of 15.0 kV) was used to observe the surface microstructure of MG, Carbon@MG and the bending fracture, wear surface morphology of MG/Cu, Carbon@MG /Cu composites. Contact angle equipment (CA-100D) was used to measure the variation of the contact angle of phenolic resin on the matrixes of MG and flake graphite (FG), respectively, with time. In the experiments, approximately 1g of

MG and FG powder was pressed into a cylinder with a certain strength, and the liquid phenolic resin was dropped onto the graphite matrix through a syringe as droplet spheres. Structural defects of MG, CMG and Carbon@MG/Cu were characterized by micro confocal Raman (LabRAM HR Evolution) with a beam range of 1200-2000 cm^{-1}, Which was performed with a 532 nm laser at 75 mW. The number of measurement points for each sample was 4. The conductivity of samples was measured by an FD101 digital portable eddy current conductivity meter (operating frequency is 60 Hz with a range of 8.6-110% IACS), and the surface was sanded with 600-2000 grit sandpaper prior to measurement to ensure a smooth surface. The hardness of materials was determined by indentation test by using micro hardness tester (HV-1000STA) on the polished surface of specimens under 48N and keeping 15s. Bending strength tests were carried out on samples machined to 80 x 10 x 8mm on a Type 304C universal testing machine. The bending strength was determined by a three-point bending test with a span of 75 mm and a limit block downward speed of 0.5 mm/min. All results are the average of at least four measurements per sample.

2.4 wear test

Graphite/Cu composites have excellent mechanical properties, wear resistance and electrical conductivity and are suitable for aerospace, transportation and other friction braking materials such as brushes, electrical contacts, bearing bushings etc. Surface contact in a sliding bearing is simulated and tribological tests are carried out in a rotary wear tester (MS-T3001, Lanzhou Huahui Instrument Technology Co., Ltd.). Fig. 2 shows a schematic diagram of the tribological wear tester, with the tribological wear

1   tester connected to a sensor, a GCr15 steel ball as a pin and the sample as a disk. The

2   surface size of the composite material is Ø20mm, for grinding small steel balls (GCr15)

3   is an effective material in sliding bearings. Graphite/Cu composites as a bearing

4   bushing with bearing material, and bearing with the work, need good mechanical

5   properties and wear resistance support. The test was conducted at room temperature

6   and the test was repeated four times for each sample, each test lasting 30 minutes.

7   Friction test data was taken from the repeated tests and standard deviations are

8   calculated. The test load was maintained at 4 N and the motor was rotated at 300 rpm.

9   The surface of the specimen was ground and polished to remove surface contaminants

10   before the tribological test. The cross-sectional area of the abrasion marks A was

11   obtained by observing the three-dimensional shape of the abrasion marks using a Mahr-

12   LD130 optical profiler, the wear volume ΔV (mm^3) was calculated from equation (1)

13   and the wear rate W was calculated from equation (2).

14
$$\Delta V = AL \quad (1)$$
15

16
$$W = \frac{\Delta V}{F_N S} \quad (2)$$

17   Where L is the length of the wear mark (mm), F_N is the normal load (N) and S is the

18   sliding distance (m). At the end of the experiment, the steel balls were not reused and

19   new balls were used to replace the old ones before the new experiment was carried out.

20   In this experiment, each friction experiment was repeated four times to ensure the

21   accuracy of the experimental data.
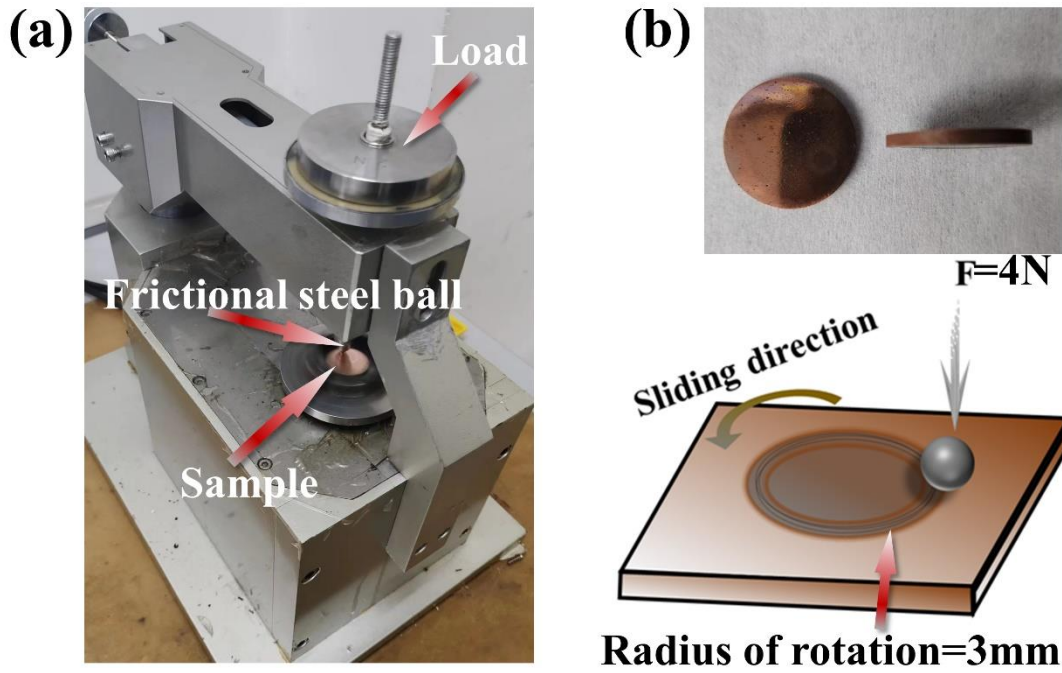
Figure 2. The schematic illustration of the wear testing machine (a), the friction sample

and the rotational friction test (b).

3. Results and discussion

3.1 The effects of carbon coating on the crystal structure of microcrystalline graphite

The variation of contact angle of liquid phenolic resin at 30°C with time for MG

and flake graphite matrixes is shown in Fig.3, Fig.3(a) is MG matrix and Fig.3(b) is

flake graphite matrix. According to Fig.3, both MG and flake graphite have good

wettability with phenolic resin at 30 °C. At 0s, the contact angles of the phenolic resin

with MG and flake graphite are 74.5° and 76.8° respectively. The contact angle

measurements lasted for a total of 100.1s. The contact angle of MG and flake graphite

with phenolic resin decreases gradually with increasing time. However, the contact

angle of the MG with the phenolic resin is always smaller than that of the flake graphite

throughout the measurement process. When 100.1s is reached, the phenolic resin

1 solution basically spreads on the MG matrix and its contact angle becomes 30.8°. As

2 can be seen from Fig. 3, the phenolic resin clearly does not spread as much on the flake

3 graphite as the MG, with a contact angle of 44.4° at the time of 100.1s. The high

4 crystallinity of the graphite structure has a negative effect on the wetting behavior of

5 the phenolic resin.MG is made up of randomly arranged grains of less than 1 μm in size.

6 Compared to flake graphite, microcrystalline graphite has small internal grain sizes and

7 the random arrangement exposes a large number of 002 crystalline surfaces. And the

8 surface of the grains contains a large number of defective structures with high reactivity,

9 so MG has good wettability with phenolic resin[18].
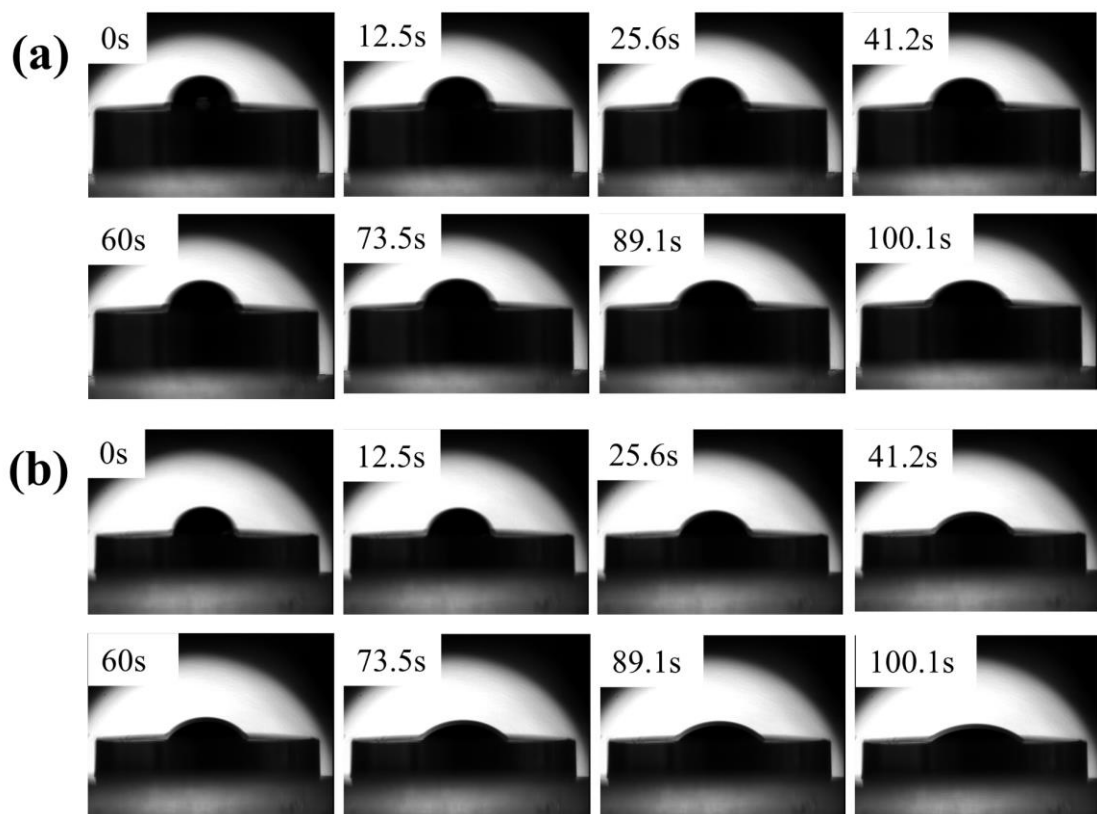
10

11 Figure 3. Variation of contact angle of liquid phenolic resin on flake graphite matrix(a)

12 and MG matrix(b) at 30°C with time.

XRD patterns of MG and Carbon@MG are shown in Fig.4(a). Both (002) and (004) crystallographic diffraction peaks of two samples are very distinct, indicating that the phenolic resin coating has not significantly altered the crystal structure of the MG. From the diffraction pattern in Fig.4(b), it can be found that the intensity of the diffraction peaks on the (002) and (004) crystal planes of the MG is reduced after phenolic resin coating and the peaks are shifted to a small angle. The graphitization degree and grain size of both samples can be calculated according to the Bragg's equation (3) and Franklin's formula (4), and the graphitization degree and grain size of both samples can be calculated using Scherrer's formula (5), and the results are shown in Table 1.

$$d_{002} = \frac{\lambda}{2 \sin \theta} (3)$$

$$\gamma = \frac{3.440 - d_{002}}{3.440 - 3.354} \times 100\% (4)$$

$$L_C = \frac{K\lambda}{\beta \cos \theta} (5)$$

where d_{002} is the graphite grain spacing in nm, γ is the degree of graphitization, L_C is the graphite grain size in nm. λ is the X-ray diffraction wavelength, a constant with a value of 0.15406 nm, θ represents the angle between the X-ray and (002) grain surfaces. k is 0.89, β is the half-height width of the highest diffraction peak of microcrystalline graphite, and the fitted β values before and after carbon cladding are shown in Table 1.

Compared to microcrystalline graphite, the phenolic resin-coated MG layer spacing increases and the graphitization degree decreases from 90.06% to 87.76%. The diffraction intensity is a superposition of the relative intensities of the different structural carbon material components and reflects the amount of different structural

carbon material components. The phenolic resin is distributed on the surface of the MG

after carbonization. It is small amorphous particles with an amorphous structure and

low graphitization, hence the reduced graphitization of Carbon@MG. The Raman

spectra of the samples are shown in Fig.4(c). The characteristic peak D located at the

wavenumber of 1360 cm^{-1} and the G peak located near 1580 cm^{-1}. Usually the intensity

of the D peak is related to the SP^3 hybridization of the carbon atoms, with larger D-

peak values indicating more defects in the carbon material[19]. The R value (R=ID/IG)

is commonly used in Raman spectroscopy to characterize the degree of disorder in

graphite, the higher the R value the higher the degree of disorder in graphite. The R

value for MG was 0.37, while the R value for Carbon@MG after the coating treatment

rose to 0.87, an increase of 57.47%. This indicates a high degree of disorder in the near-

surface region of Carbon@MG, apparently due to the coating of an amorphous layer of

carbon on the MG surface. The R values for MG and Carbon@MG are 0.37 and 0.87

respectively, which are in good agreement with the XRD results.
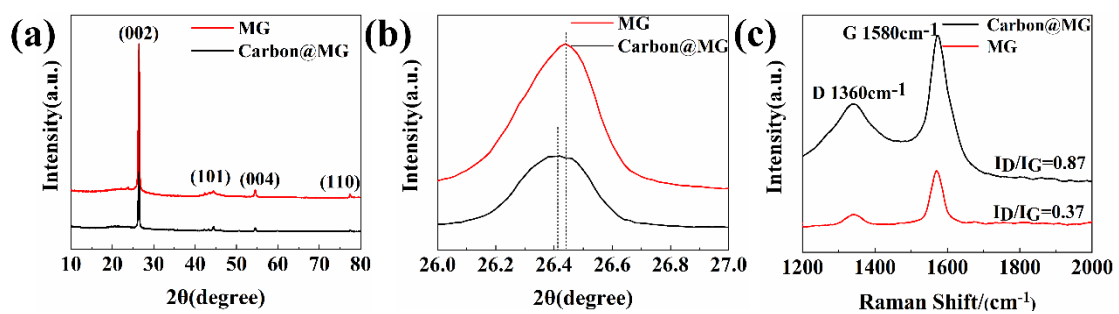
Figure 4. XRD patterns(a) and Raman spectra(c) of MG and Carbon@MG, where (b)

is a magnified view of a at 26-27°.

Table 1 The d_{002}, γ, L_C and β of samples

|	d_{002}/nm	γ /%	L_C/nm	β
MG	0.3399	90.06	23.5979	0.34
Carbon@MG	0.3424	87.76	23.5883	0.31

3.2 Effect of carbon coated on microstructure of MG

The microstructures of MG, PR@MG and Carbon@MG are illustrated in Fig.5. As shown in Fig.5(a), MG consists of a disordered arrangement of tiny lamellar particles with a loose morphology, which are not uniform in size, ranging from a few microns to tens of microns. The SEM image of the MG at high magnification are illustrated in Fig.5(a-1). The surface of the microcrystalline graphite is rough and accompanied by cracks, and there are some irregular nanoflakes that are not tightly bonded to the substrate, these weakly bonded graphite nanoflakes may fall off from the main body in friction wear, affecting the friction performance. The morphology of the PR@MG is shown in Fig. 5(b)&(b-1). The surface roughness and cracks of the MG are significantly reduced, many unstable structures and sites are covered, showing a relatively smooth surface, and the microstructure of the graphite layer stacks becomes blurred for some levels. Fig.5(c)&(c-1) shows the surface morphology of Carbon@MG, where the phenolic resin is transformed into a smooth layer of amorphous carbon covering the graphite surface after high temperature carbonization. This amorphous carbon with lattice defects and stacked lamellar dislocations, composed of SP^2 and SP^3 hybridized carbon atoms, has high mechanical strength. Fig.5(d) presents the TEM diffraction pattern of the resin-coated MG before carbonization (PR@MG), the thickness of the coating layer on the surface of the MG is 150 nm. After carbonization the thickness of

the coating layer decreases and there is a clear graphite electron diffraction pattern in the inner layer. The loss of thickness of the resin coating is caused by thermal fragmentation and decomposition of the resin skeleton during the carbonization phase (~900°C), including the volatilization of water, volatile substances (e.g., phenol derivatives and aromatics) and gaseous molecules (e.g.CO, CO_2 or H_2)[20, 21]. The transmission electron micrograph of Carbon@MG is shown in Fig.6(a), from which it can be seen that the surface of the microcrystalline graphite has a resin coating layer with a thickness of approximately 30 nm, and the coating layer is well bonded to the graphite. The inner graphite layer in Figure 6(b) is crystalline and the transmission electron diffraction pattern shows a hexagonal structure. Figure 6(c) shows the outer resin diffraction pattern with amorphous carbon in the outer layer, no diffraction pattern is observed.
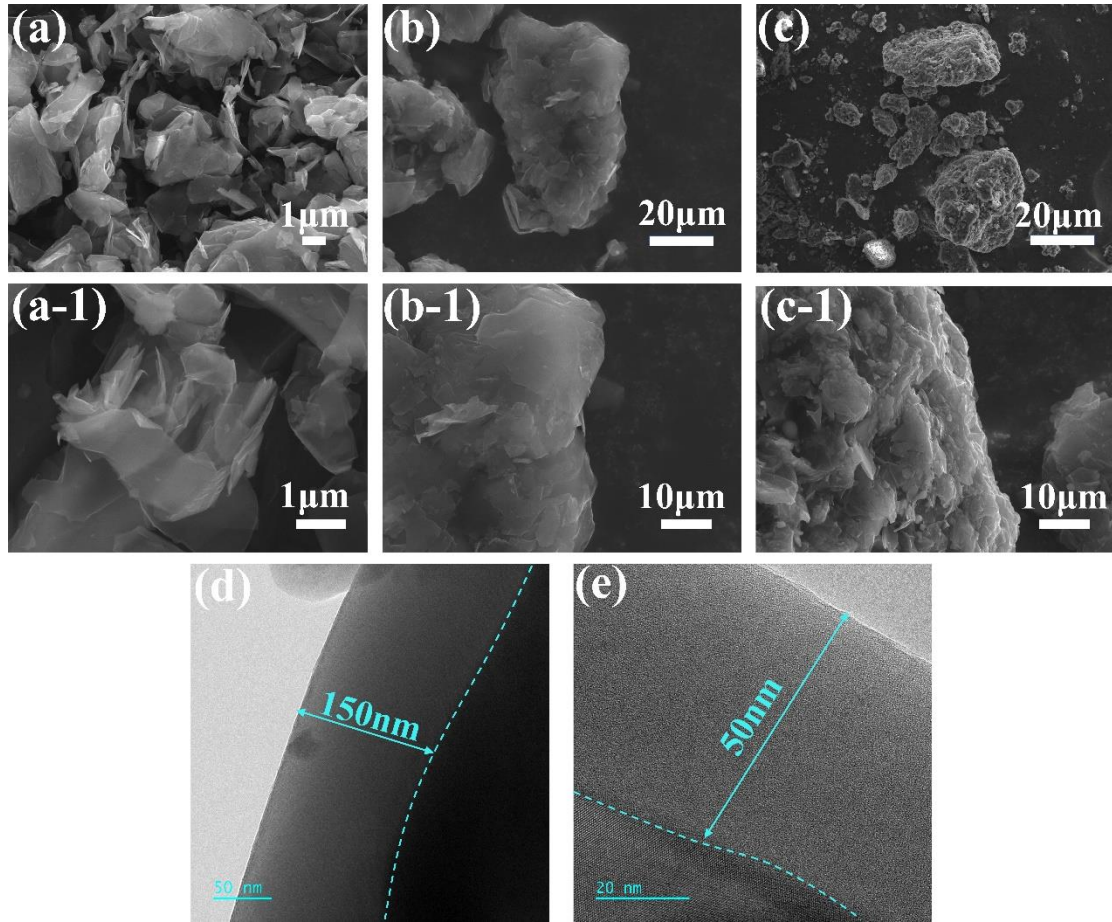
Figure 5. SEM images of MG (a, a-1), PR@MG (b, b-1) and Carbon@MG (c, c-1),

TEM images of PR@MG(d) and Carbon@MG(e).
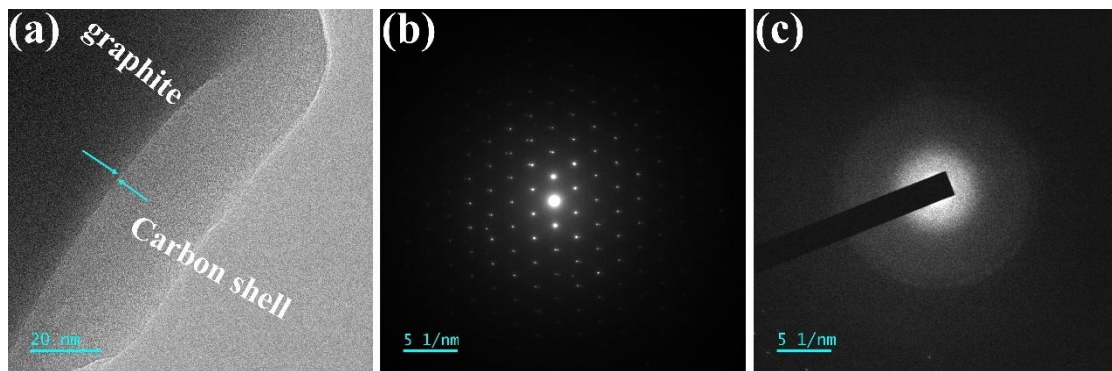
Figure 6. TEM images of Carbon@MG(a), electron diffraction patterns of inner

graphite(b) and outer resin(c).

3.3 The physical and mechanical properties of composites

The physical and mechanical properties data for the pure Cu, MG/Cu and Carbon@MG/Cu samples are summarized in Table 2. The addition of graphite to the copper matrix resulted in a decrease in the relative density and conductivity of the composite. The relative density of MG/Cu is 70.3%, a decrease of 26.2% relative to pure Cu. On the one hand, poor interfacial bonding between Cu and graphite, graphite/Cu composite form a pseudo-alloy, and internal defects in the composite prevent complete sintering of the matrix. On the other hand, the graphite is diffusely distributed in the Cu matrix, which hinders the migration of Cu particles during the sintering process, and the internal pores of the material cannot be excluded, so the relative density decreases. The conductivity of graphite is much lower than that of Cu. The mechanism of conductivity of pure Cu is the directional movement of electrons, and the addition of graphite destroys the integrity of the matrix lattice, generating a large number of dislocations and lattice distortions near the copper grain boundaries to increase the chance of electron scattering, so the conductivity of the composites will also decrease after the addition of graphite. However, the relative density and conductivity of the Carbon@MG composite increases. Resin-coated MG improves the interfacial bonding between the MG and Cu, fills the internal pores of the composite matrix and the Cu particles form an interconnected conductive network. During the carbonization stage, the phenolic resin also emits some reducing gases such as CO, H_2 and CH_4 to break the oxide film on the surface of the Cu particles and promote the sintering and sintering of the Cu particles. Compared to pure Cu, the hardness and bending strength of MG/Cu are both reduced. The hardness of Carbon@MG/Cu

reached 72.3 HV, increased by 139.4%, and the bending strength increased by 96.2%. Graphite is a textured soft phase, and the distribution of graphite in the Cu matrix can be regarded as pores cutting through the matrix, so the hardness and flexural strength of MG/Cu composites are reduced. However, Carbon@MG is more closely bonded to the copper matrix and effectively fills the internal pores.

Figure 7 illustrates the bending fracture morphology of the three materials. Pure Cu shows typical ductile fracture characteristics. The fracture surface is distributed with dimples larger than those with different depths, showing typical ductile fracture traces. The bending fracture pattern of MG/Cu is shown in Fig. 7(c), where the cracks tend to extend along the graphite enriched areas and graphite strips are present on the fracture surface, with the graphite poorly bonded to the copper and large substrates being pulled out under bending load, resulting in large holes and pits on the fracture surface. The flexural fracture of Carbon@MG/Cu has some signs of ductile fracture, with the graphite phase alternating with the copper phase. The Carbon@MG shows higher densities, and Carbon@MG is pulled off in the bending test leaving some graphite fragments, which indicates that it is more tightly bonded with the Cu matrix interface, and no serious fracture and crack extension are seen. For the MG/Cu, the bending fracture shows large cracks and many fine cracks with MG fragments. The poor densification of MG/Cu, natural defects of MG and detachment of graphite flakes during the mixing process have affected the continuity of the Cu matrix. Lacking the protection of amorphous carbon shell, the interlayer force of graphite is very small, and a very small force will break the MG. Therefore, without the protection of amorphous

carbon shell, the main crack breaks through the interlayer force of MG under stress and

extends rapidly through the interior of MG, and a part of cracks passes through these

pores and cracks rapidly and splits the Cu matrix. This will lead to rapid fracture of

MG/Cu. Destruction of MG by external forces and poor bonding between Cu matrix

and MG will lead to shedding and loss of MG in the matrix. This suggests that the Cu

matrix does not fix the MG during friction, resulting in a non-uniform distribution of

the lubricant film. The intact Carbon@MG is well bonded to the Cu matrix, and no

cracks are generated inside the Carbon@MG protected by the amorphous carbon shell.

The main cracks are extended along the Carbon@MG interface, pulling out or breaking

the Carbon@MG, a process that consumes a large amount of energy and significantly

enhances the mechanical properties of the composites. Therefore, Carbon@MG/Cu are

able to withstand higher loads, and the amorphous carbon shell not only protects the

integrity of Carbon@MG, but also in the crack extension, the crack extends along the

Carbon@MG-Cu interface as well as the dense-body Cu-Cu interface, which consumes

more energy, and the composite material undergoes a continuous and slow fracture

under the external force.

Table 2 The physical and mechanical properties of composites

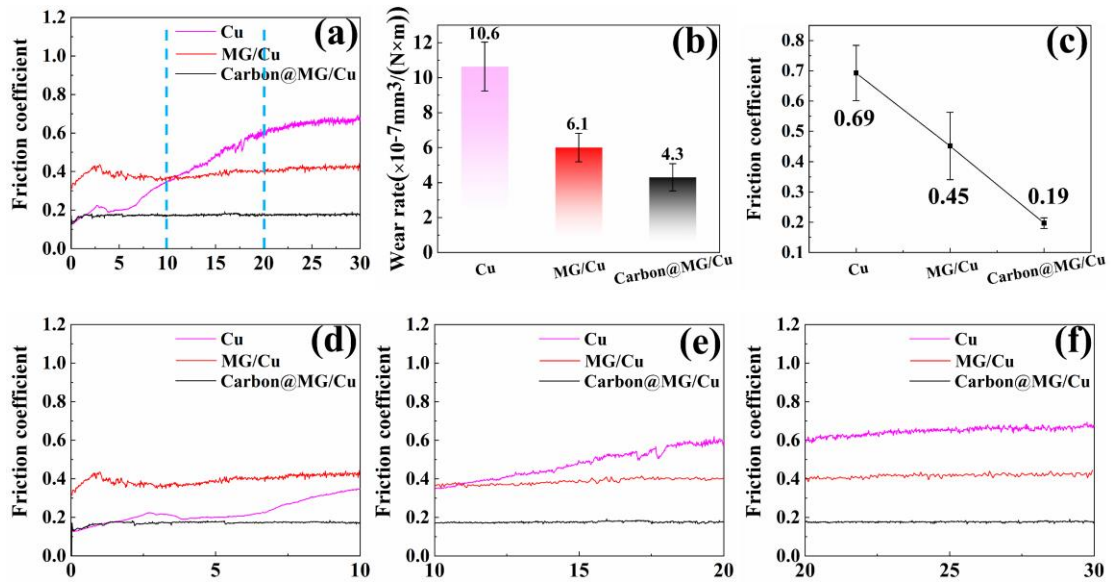| Materials	Relative density (%)	Hardness (HV)	Flexural strength (MPa)	Conductivity(%IACS)
Pure Cu	95.2	39.8	60.2	95.6%
MG/Cu	70.3	30.2	52.9	85.1%
Carbon@MG/Cu	90.5	72.3	103.8	90.3%
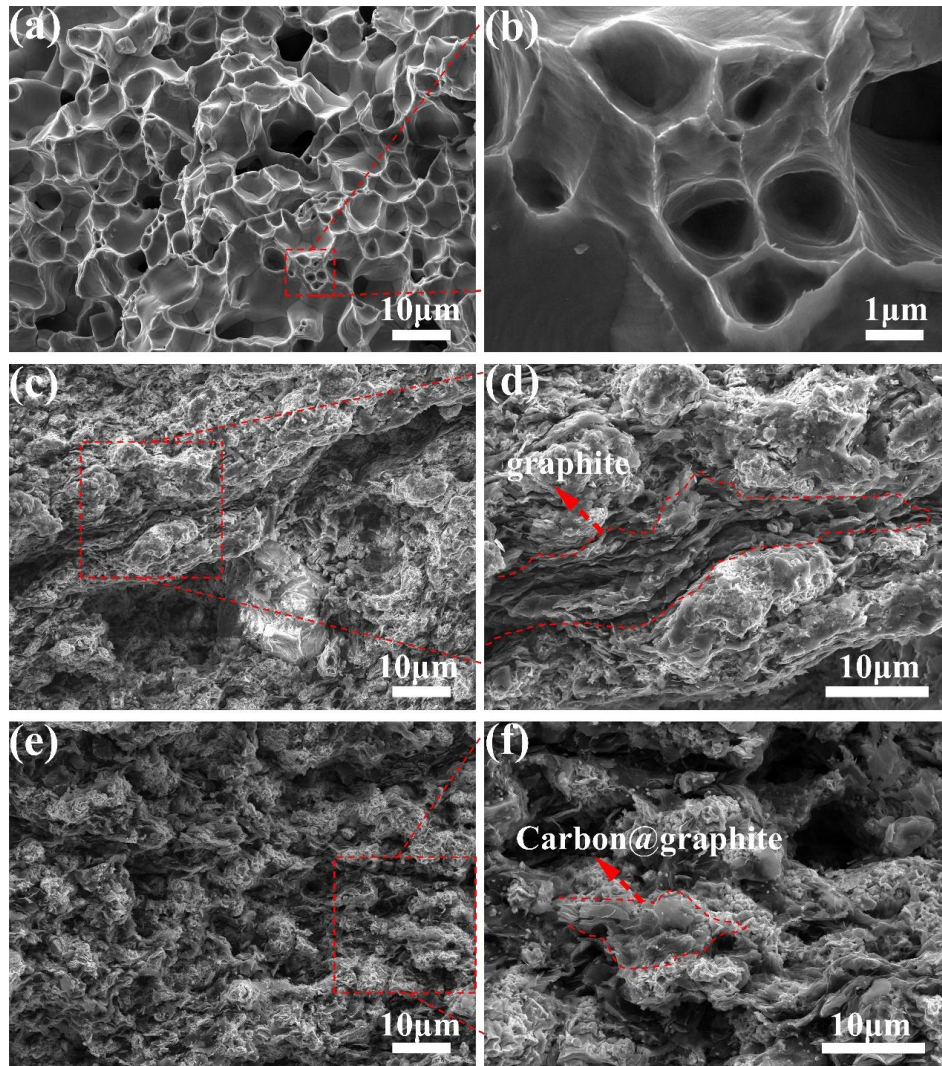
Figure 7. The fracture morphologies of pure Cu(a), MG/Cu(c) and Carbon@MG/Cu(e), where b, d and f are partial enlargements of a, c and e respectively.

3.4 Friction coefficient and wear rate of composites

The friction coefficient of the composites as a function of time and the results of the wear rate are shown in Fig. 8. The friction coefficient of pure Cu is high, with an average friction coefficient of 0.69. The friction coefficient of pure Cu shows an overall increasing trend, as shown in Fig. 8(d), (e) and (f). The addition of graphite lubricant phase to the Cu matrix reduces the friction coefficient. The friction coefficient of Carbon@MG/Cu composite is the lowest, at 0.19, which is 72.4% less than that of pure

1　Cu. In order to compare the friction coefficient fluctuation levels of pure Cu, MG/Cu

2　and Carbon@MG/Cu composites, the standard deviation of friction coefficients was

3　calculated for each of the three groups of samples in Fig. 8(c). The larger the standard

4　deviation, the more the coefficient of friction fluctuates and the coefficient of friction

5　is in an unstable state. The standard deviation of the coefficient of friction is 0.09 for

6　pure Cu and 0.11 for MG/Cu. The standard deviation of the coefficient of friction for

7　Carbon@MG/Cu is 0.017, which is 84.5% lower than MG/Cu. As shown in Fig. 8(b),

8　the wear rate of pure Cu is 10.6 x 10^{-7} (mm^3 /(N·m)), while the wear rate of MG/Cu

9　composite is reduced to 6.1 x 10^{-7} (mm^3 /(N·m)), and the wear rate of Carbon@MG/Cu

10　composite is the lowest at 4.3 x 10^{-7} (mm^3 /(N·m)), which is 59.4% lower than that of

11　pure Cu. When pure Cu is in direct contact with a small steel ball, adhesion and cold

12　welding occur at the contact surface, and the absence of a lubricating phase leads to a

13　high wear rate and an unstable friction coefficient. the higher hardness of the

14　Carbon@MG/Cu composite and the higher interfacial bonding strength between

15　Carbon@MG and the Cu matrix reduce the risk of matrix detachment during friction

16　and effectively reduce the wear rate. Carbon@MG/Cu have a smooth change in friction

17　coefficient and the lowest wear rate, which is related to the fact that the amorphous

18　carbon shell protects the graphite flakes from detachment and thus forms a complete

19　and continuous lubrication film. The surface of the composite is able to form a more

20　complete lubricating film and the matrix is harder and more wear resistant[22].

Fig 8. Variation of the friction coefficient of the composite material with time (a) and local enlargements for each time period ((d), (e) and (f)), wear rate (b) and average friction coefficient (c).

Table 3 compares the coefficient of friction and wear rate of Carbon@MG/Cu composites obtained in this study with the coefficient of friction and wear rate of (Ag, Cu, Al)-Graphite and other materials reported in related literature. It can be clearly observed that the wear rates of Ag-Graphite, Cu-Graphite and other composites reported in the relevant literature are greater than 10^{-6} (mm^3 /(N·m)).In this study, Carbon@MG/Cu has a wear rate as low as 4.3 x 10^{-7} (mm^3 /(N·m)) , which is not in an order of magnitude with the results reported in the related literature, and is even smaller than that of the Cu-based material reinforced by high-strength graphene (GNS) (0.5 × 10^{-5} (mm^3 /(N·m))). This suggests that graphite/Cu composites with more excellent friction and wear properties can be obtained by using carbon-coated microcrystalline graphite as the lubricating phase.

Table 3 Comparison of friction coefficients and wear rates of different composites.

Materials	method	Coefficient	Wear rate	Reference
10%Gr/CBCCS	MLM	0.2-0.3	5.5×10^{-5}	[23]
Foam copper-graphite/copper	MLM	0.225	0.21×10^{-6}	[24]
Ag/graphite	MLM	-	1.6×10^{-6}	[25]
20%high-content graphene/Cu	MLM	-	0.5×10^{-5}	[26]
15%Graphite/Cu663	MLM	0.1	1.5×10^{-5}	[27]
25%MCMB/Cu	MLM	0.2	0.5×10^{-4}	[28]
Cu@graphite/Cu	electrical explosion method	0.5-0.6	5.46×10^{-3}	[29]
Cu-Ni-Graphite4%	MLM	0.153	0.1151×10^{-3}	[30]
Ni/Al-Cu/GNS	Colloid method	0.65	9×10^{-5}	[31]
★This study Carbon@MG/Cu	MLM	0.19	4.3×10^{-7}	

3.5 Wear morphology and mechanism

The SEM morphology of the wear surface of the composites after 30 minutes of friction is shown in Fig. 9. The wear surface of pure Cu shows mainly grooves with surface delamination and furrows (Fig. 9a). The depth of the grooves and the area of delamination are relatively large, and the furrow marks are more obvious. The repeated accumulation of stresses and frictional heat between the friction pairs cannot be released, and there is no lubricating film on the contact surfaces. Adhesion and cold welding occur between the friction subs, the pure Cu surface is dislodged under the action of cyclic frictional stresses and large pits appear on the wear surface. At the same time the pure Cu surface adhering to the counter-abrasive body is transformed into

abrasive grains, which slide under shear to produce plough grooves. This indicates that

the wear mechanism of pure Cu is abrasive wear. It is generally accepted that abrasive

wear is caused by hard particles embedded in the surface. Under load, the surface of the

weak substrate shows signs of furrow wear. The degree of abrasive wear is related to

the difference in hardness between the two friction surfaces[19]. Pure Cu is less hard

and wear surface abrasive traces are more pronounced. The results of the EDS sweep

of the spalling pits in Fig. (a-1) show that severe oxidation has occurred on the pure Cu

wear surface, with an oxygen content of 7.56%. The spalling pits are the result of the

shedding of oxidation products. Oxidative wear and abrasive wear occur mainly on pure

Cu. Severe wear of pure Cu also occurs on the grinding balls and is transferred to the

disc surface, which is confirmed by the elemental Fe in the EDS analysis. There is no

lubricating film present between the pure Cu friction pairs and the frictional heat causes

oxidative wear on the pure Cu surface. The addition of MG to the Cu matrix

significantly altered the wear morphology with little delamination and spalling seen on

the surface of the MG/Cu, and plough marks were very evident, indicating that MG/Cu

mainly experience abrasive wear. EDS analysis of the wear surface shows a slight

elemental Fe content on the wear surface of the MG/Cu. This indicates that the presence

of a lubricating film effectively protects the counter body against wear. In addition to

the obvious plough marks, pits and large abrasive chips can be seen on the surface of

the MG/Cu. Some oxidation inclusions on the surface of the sample restrict the slip and

movement of the matrix dislocations, resulting in stress concentrations on the wear

surface, and the bond strength between the MG and Cu matrix is low. The surface of

1 Carbon@MG/Cu shows no obvious signs of ploughing or spalling, and the wear surface

2 is significantly smoother in appearance. The wear surface has a relatively homogeneous

3 distribution of C elements and no Fe elements are detected in the counter body, which

4 indicates that the counter body is effectively protected against wear. This indicates that

5 only slight plastic deformation of the Carbon@MG/Cu composites surface has occurred.

6 When plastic deformation of the material on the contact surface is prevented, the wear

7 rate can be minimized[32]. Slight abrasive wear is the wear mechanism of the

8 Carbon@MG/Cu composite. Fig.10(a-c) show the 3D wear profile of the samples.

9 From Fig.10(a) it can be seen that the pure Cu wear marks are wider and the wear marks

10 are deeper. The wear marks of the MG/Cu are shallower and smoother. The plough

11 marks on the wear surface of the Carbon@MG/Cu are significantly reduced and the

12 wear marks are the shallowest, indicating that the Carbon@MG/Cu have excellent anti-

13 wear properties.

14
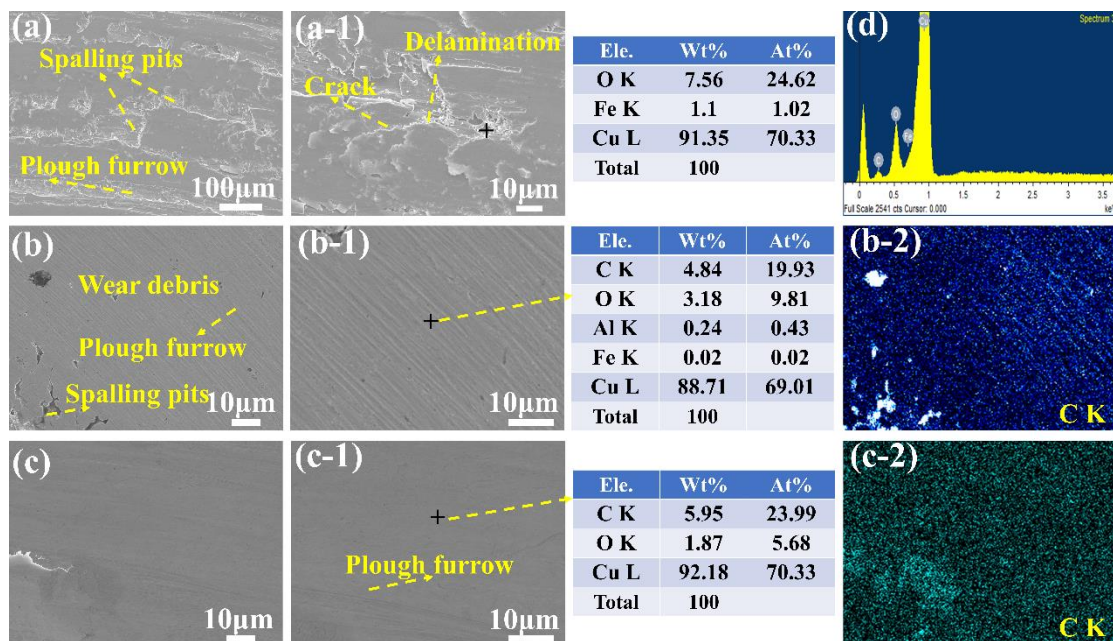
Figure 9. SEM images of the wear morphology of pure Cu, MG/Cu and Carbon@MG/Cu and local enlargements (a-1, b-1, c-1), (b-2) and (c-2) for (b), (c) EDS analysis respectively.
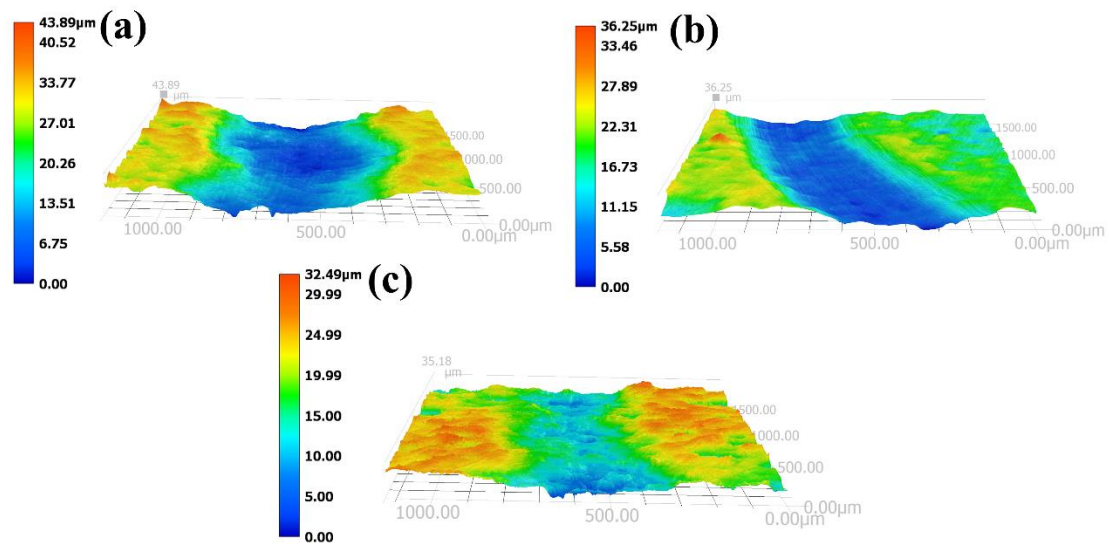
Figure 10. 3D profile of the wear surface of pure Cu(a), MG/Cu(b) and Carbon@MG/Cu(c).

The wear microscopy and the corresponding EDS elemental distribution of the Pure Cu, MG/Cu and Carbon@MG/Cu composites are shown in Fig. 11. The wear surface of the Pure Cu counter-grind has a Cu film transferred from the Cu matrix and adhesion between the contact surfaces. In addition, many plough marks were found on the counter-grinding counter body, with more severe abrasive wear. Fig. 11(b) shows the microscopic morphology of the MG/Cu counter-grind. The surface of the small steel ball is covered with a carbon film, which is transferred from the wear surface of the MG/Cu. The carbon film on the surface of the small steel ball is incomplete, and the carbon film in Fig. 11(b) shows extended cracks. As can be seen from the EDS results (Fig. 11b-2), the transfer film on the surface of the small steel ball is not complete and continuous over the surface, and many plough marks are also found on its surface. This

1 indicates that the counter-abrasive counter body of MG/Cu underwent abrasive wear. A

2 carbon-rich transfer film and slight furrow marks were also observed on the

3 Carbon@MG/Cu counterpart (Fig. 11c). However, this transfer film is continuous and

4 intact, effectively protecting the Carbon@MG/Cu counterpart.

Ele.	Wt.%	At.%
C K	9.07	32.05
Cr K	1.59	1.30
Fe K	75.42	57.35
Cu K	13.92	9.30
Total	100	
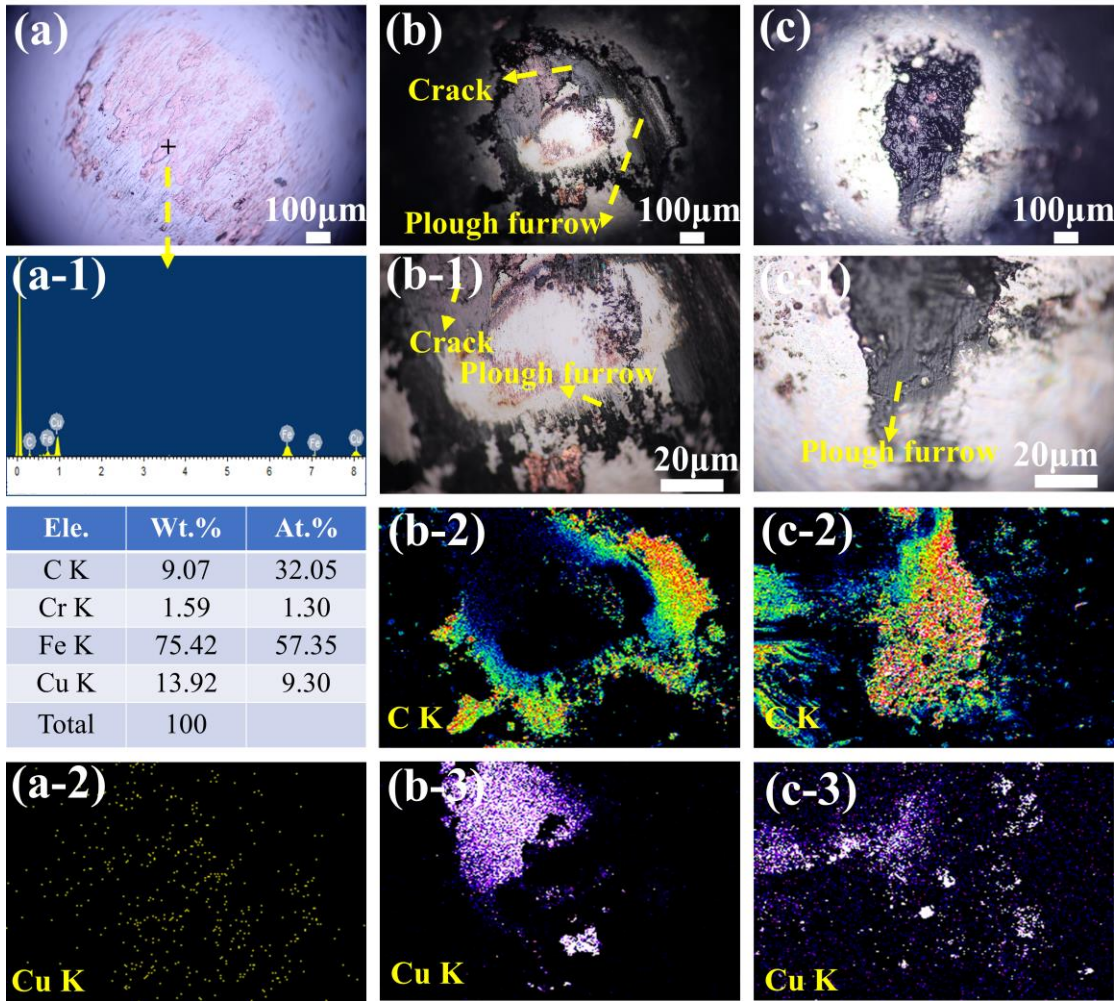
6 Figure 11. Wear morphology of pure Cu(a), MG/Cu (b, b-1) and Carbon@MG/Cu (c,

7 c-1) against grinding antimatter and the corresponding EDS analysis.

8   The wear mechanism of self-lubricating composites of different materials is shown

9 in Fig.12. Pure Cu in sliding, direct contact between the frictional matrix, the frictional

10 matrix repeatedly between the frictional wear generates stress and frictional heat cannot

11 be released. Adhesion occurs due to local cold welding between the highest points of

the friction surface, the dislodged Cu matrix adheres to the small ball scratching the friction surface and cracks extend in the matrix. With the addition of graphite, the composite undergoes plastic deformation to extrude the graphite from the Cu matrix onto the counter-abrasive surface to improve the wear resistance of the composite. However, the graphite is poorly bonded to the Cu interface and there are many holes within the material. Under high loads and high friction, cracks expand along the graphite-Cu interface, destroying the continuity of the matrix, and the MG/Cu composite is unable to lubricate the friction surface. Abrasive debris generated by the composite during sliding destroys the integrity of the lubricating film on the friction surface and therefore the wear resistance of the MG/Cu composite is poor. The modified MG is more closely bonded to the Cu matrix and the internal structure of the matrix is continuous, providing continuous lubrication to the friction surface to form a more complete lubrication film.
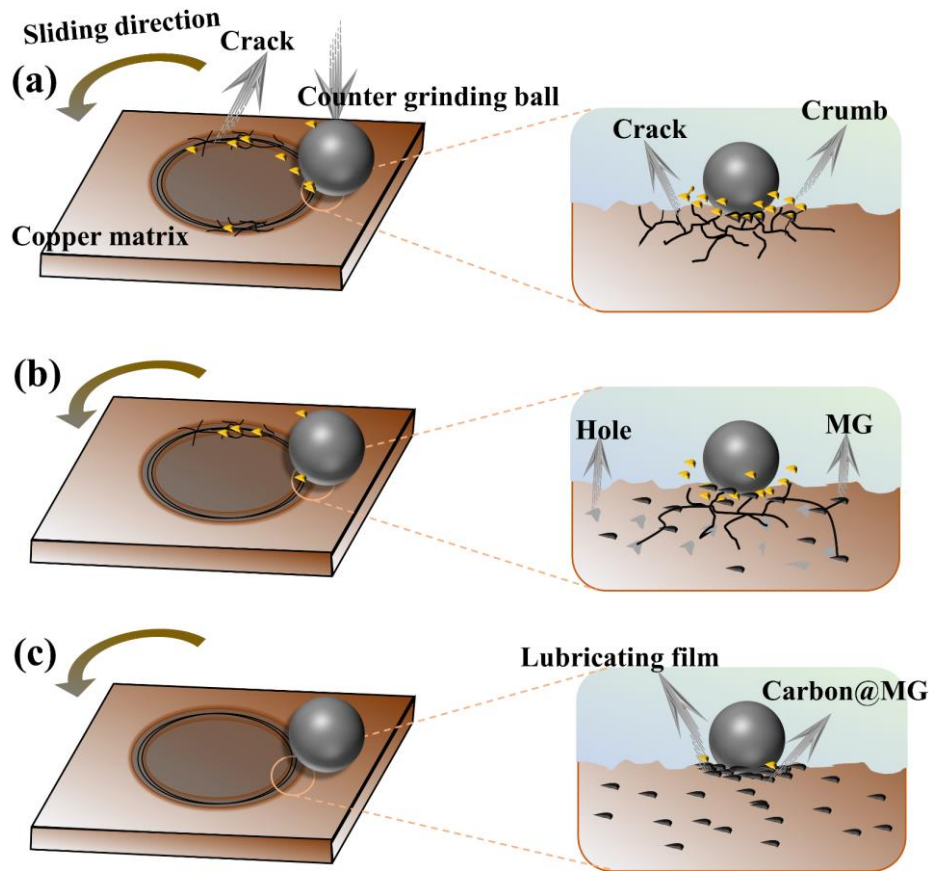
Figure 12. Wear mechanism illustration for pure Cu(a), MG/Cu(b) and Carbon@MG/Cu(c).

4. Conclusions

In conclusion, this study developed a novel Carbon@MG/Cu composites with good mechanical and tribological properties by coating modified MG with phenolic resin. The effect of the modified graphite on the tribological and mechanical properties of the composites was investigated in detail. The results shown that the phenolic resin binds well to the MG and forms a carbon shell with a certain thickness on the surface of the MG after carbonization. The mechanical properties of Carbon@MG/Cu are greatly improved compared to pure Cu and MG/Cu. The hardness and flexural strength of Carbon@MG/Cu reached 72.3 HV and 103.8 MPa, 81.6% and 72.4% increase

compared to MG/Cu respectively. The resin-coated modified MG improves the interfacial bonding between graphite and Cu, and the Cu particles form a connected conductive network to improve the electrical conductivity of the composite. At the same time, the friction coefficient of Carbon@MG/Cu decreases sharply (0.19), and the fluctuation of the friction coefficient is small, which can be attributed to the formation of a more complete lubrication layer at the contact interface of the friction pair. In addition, due to the self-healing function of Carbon@MG, its wear rate is only 4.3×10^{-7} (mm^3/(N·m)). Carbon@MG reduces the wear (about 30-60%). Pure Cu is soft and prone to abrasive and adhesive wear under the action of friction balls. In addition, the heat generated between the friction partners causes severe oxidative wear of pure Cu. MG/Cu is embedded in the surface by micro-convex bodies during friction due to its low hardness, causing abrasive wear. The friction contact surface of MG/Cu generates an incomplete and discontinuous lubricant, which slightly reduces the heat in the friction process, resulting in a slight oxidative wear. The mechanical properties of Carbon@MG are significantly improved and no significant abrasive wear is observed. A complete and continuous lubrication film between the friction partners effectively protects the composite material and the anti-wear balls.

Funding

Declarations

Competing interests. The authors declare no competing interests.

Authors' Contributions:

M.Zhong and S. Duan conducted the experiments, M.Zhong, X.Wu and B.Luo wrote the manuscript. X.Min, Z.Huang, M.Fang, H.Li and H.Ding analysed the results. All authors reviewed the manuscript.

References

[1] N. Cui, L. Sun, L. Bagas, K. Xiao, J. Xia, Geological characteristics and analysis of known and undiscovered graphite resources of China, Ore Geology Reviews 91 (2017) 1119-1129.

[2] X.-l. Liu, Z.-b. Cai, Q. Xiao, M.-x. Shen, W.-b. Yang, D.-y. Chen, Fretting wear behavior of brass/copper-graphite composites as a contactor material under electrical contact, International Journal of Mechanical Sciences 184 (2020).

[3] C. Salvo, R.V. Mangalaraja, R. Udayabashkar, M. Lopez, C. Aguilar, Enhanced mechanical and electrical properties of novel graphene reinforced copper matrix composites, Journal of Alloys and Compounds 777 (2019) 309-316.

[4] X. Zhou, L. Chen, H. Cao, J. Yu, G. Qiu, L. Wang, Effects of emulsified asphalt on the mechanical and tribological properties of copper/graphite composites, Materials Research Express 6(5) (2019).

[5] Y. Wei, Y. Jiang, N. Li, Z. Hu, X. He, X. Ouyang, Analysis on microcrystalline graphite and properties of MgO-C refractories with microcrystalline graphite, Advances in Applied Ceramics 114(8) (2015) 423-428.

[6] X. Tong, Z. Bai, J. Wu, Mechanical and tribological performance of acrylonitrile-butadiene rubber/carbon black/cryptocrystalline graphite composites, Journal of Applied Polymer Science 138(9) (2021).

[7] D.H. He, R. Manory, A novel electrical contact material with improved self-lubrication for railway current collectors, Wear 249(7) (2001) 626-636.

[8] Y.Z. Zhan, G.D. Zhang, Y.Y. Wu, Effect of surface metallization of graphite on the tribological properties of copper hybrid composites, Scandinavian Journal of Metallurgy 33(2) (2004) 80-84.

[9] A. Mazloum, J. Kovacik, S. Emmer, I. Sevostianov, Copper-graphite composites: thermal expansion, thermal and electrical conductivities, and cross-property connections, Journal of Materials Science 51(17) (2016) 7977-7990.

[10] L. Chen, G. Yu, Y. Chu, J. Zhang, B. Hu, X. Zhang, Effect of three types of surfactants on fabrication of Cu-coated graphite powders, Advanced Powder Technology 24(1) (2013) 281-287.

[11] H. Xu, J.-h. Chen, S.-b. Ren, X.-b. He, X.-h. Qu, Sintering behavior and thermal conductivity of nickel-coated graphite flake/copper composites fabricated by spark plasma sintering, International Journal of Minerals Metallurgy and Materials 25(4) (2018) 459-471.

[12] J. Cheng, X. Gan, S. Chen, Y. Lai, H. Xiong, K. Zhou, Properties and microstructure of copper/nickel-iron-coated graphite composites prepared by electroless plating and spark plasma sintering, Powder Technology 343 (2019) 705-713.

[13] P.-H. Uk, T.-J. Chung, H. Lee, Preparation of copper-plated graphite powder, and the sintering behavior of its composite with copper, Journal of Ceramic Processing Research 18(6) (2017) 440-444.

[14] H. Zhao, L. Liu, Y. Wu, W. Hu, Investigation on wear and corrosion behavior of Cu-graphite composites prepared by electroforming, Composites Science and Technology 67(6) (2007) 1210-1217.

[15] W. Zhou, M. Yi, K. Peng, L. Ran, Y. Ge, Preparation of a C/C-Cu composite with Mo2C coatings as a modification interlayer, Materials Letters 145 (2015) 264-268.

[16] Y. Wang, Y. Gao, J. Takahashi, Y. Wan, M. Li, B. Xiao, Y. Zhang, X. He, Investigation of modification of Cu-Ni-graphite composite by silver, Materials Chemistry and Physics 239 (2020).

[17] J. Chen, S. Ren, X. He, X. Qu, Properties and microstructure of nickel-coated graphite flakes/copper composites fabricated by spark plasma sintering, Carbon 121 (2017) 25-34.

[18] K. Li, K. Shen, Z.-H. Huang, W. Shen, G. Yang, J. Yang, F. Kang, Wettability of natural microcrystalline graphite filler with pitch in isotropic graphite preparation, Fuel 180 (2016) 743-748.

[19] J.-f. Li, L. Zhang, J.-k. Xiao, K.-c. Zhou, Sliding wear behavior of copper-based composites reinforced with graphene nanosheets and graphite, Transactions of Nonferrous Metals Society of China 25(10) (2015) 3354-3362.

[20] S. Wang, X. Jing, Y. Wang, J. Si, High char yield of aryl boron-containing phenolic resins: The effect of phenylboronic acid on the thermal stability and carbonization of phenolic resins, Polymer Degradation and Stability 99 (2014) 1-11.

[21] J.-S. Yeo, J.-H. Lee, S.-H. Hwang, Effects of lignin on the volume shrinkage and mechanical properties of a styrene/unsaturated polyester/lignin ternary composite system, Composites Part B-Engineering 130 (2017) 167-173.

[22] S. Ma, E. Xu, Z. Zhu, Q. Liu, S. Yu, J. Liu, H. Zhong, Y. Jiang, Mechanical and wear performances of aluminum/sintered-carbon composites produced by pressure infiltration for pantograph sliders, Powder Technology 326 (2018) 54-61.

[23] H.J. Ling, Y.J. Mai, S.L. Li, L.Y. Zhang, C.S. Liu, X.H. Jie, Microstructure and improved tribological performance of graphite/copper-zinc composite coatings fabricated by low pressure cold spraying, Surface and Coatings Technology 364 (2019) 256-264.

[24] L. Zhu, M. Yi, L. Wang, S. Chen, Effects of foam copper on the mechanical properties and tribological properties of graphite/copper composites, Tribology International 148 (2020) 106164.

[25] Y. Sun, Y. Wang, Y. Li, K.-c. Zhou, L. Zhang, Tribological behaviors of Ag−graphite composites reinforced with spherical graphite, Transactions of Nonferrous Metals Society of China 30(8) (2020) 2177-2187.

[26] G. Lin, Y. Peng, Z. Dong, D.-B. Xiong, Tribology behavior of high-content graphene/nanograined Cu bulk composites from core/shell nanoparticles, Composites Communications 25 (2021).

[27] Y. Su, Y. Zhang, J. Song, L. Hu, Tribological behavior and lubrication mechanism of self-lubricating ceramic/metal composites: The effect of matrix type on the friction and wear properties, Wear 372 (2017) 130-138.

[28] H.-X. Guo, J.-F. Yang, Fabrication and Tribological Properties of Mesocarbon Microbead–Cu Friction Composites, Materials, 2020.

[29] H. Tan, Y. Guo, D. Wang, Y. Cui, The development of a Cu@Graphite solid lubricant with excellent anti-friction and wear resistant performances in dry condition, Wear 488-489 (2022) 204181.

[30] Y. Wang, Y. Gao, L. Sun, Y. Li, B. Zheng, W. Zhai, Effect of physical properties of Cu-Ni-graphite composites on tribological characteristics by grey correlation analysis, Results in Physics 7 (2017) 263-271.

[31] F. Yanhan, F. Jianhua, L. Ping, G. Kecheng, S. Shuang, W. Jiang, J. Zeqi, Preparation and tribological behaviors of plasma sprayed NiAl-Cu/graphite nanosheets composite coating, Tribology International 167 (2022) 107360.

[32] Y. Liu, X. Liu, X. Zhang, X. Chen, J. Zhang, L. Jing, Y. Wu, S. Yu, Tribological properties and self-lubrication mechanism of in-situ grown graphene reinforced nickel matrix composites in ambient air, Wear 496 (2022).